



## SEEDED GROWTH SYNTHESIS OF GOLD NANORODS FOR PHOTOTHERMAL APPLICATION

Do Thi Hue<sup>1,2</sup>, Vu Thi Thuy Duong<sup>1</sup>, Nguyen Trong Nghia<sup>1</sup>,  
Tran Hong Nhung<sup>1</sup>, Nghiem Thi Ha Lien<sup>1,\*</sup>

<sup>1</sup>*Institute of Physics, VAST, 18 Hoang Quoc Viet, Cau Giay, Ha Noi, Viet Nam*

<sup>2</sup>*Graduate University of Science and Technology, VAST, 18 Hoang Quoc Viet, Cau Giay, Ha Noi, Viet Nam*

\*Email: [haliem@iop.vast.vn](mailto:haliem@iop.vast.vn)

Received: 22 February 2017; Accepted for publication: 10 January 2018

**Abstract.** In this paper, the gold nanorods (GNRs) were synthesized via a seed-mediated method by using 1-3 nm seeds-in diameter and gold atoms created from the reduced Au<sup>3+</sup> ions by ascorbic acid (AA) in the presence of cetyltrimethyl ammonium bromide (CTAB) as a soft template. The aspect ratio of GNRs as well as growth yield were controlled by adjusting the concentration of Ag<sup>+</sup> ions. This method gave the formation of mono-dispersed GNRs with the controlled size and peak plasmon resonance. The UV-VIS-NIR absorption spectra and transmission electronic microscopy (TEM) images of the GNR solution showed that the plasmon absorption spectra depend on the aspect ratio of GNRs. The GNRs were also attached with bioconjugate molecules in order to be more stable and used in biomedical applications. This work also presents the results of photothermal effects of GNRs in real tissues by changing the power density of laser beam.

**Keywords:** gold nanorods (GNRs), plasmon absorption, photothermal effect, seed-mediated method.

**Classification numbers:** 2.1.1; 2.4.3; 2.2.10.

### 1. INTRODUCTION

GNRs show different colors depending on the aspect ratio, which is due to the two intense surface plasmon resonance peaks (longitudinal surface plasmon peak and transverse surface plasmon peak) corresponding to the oscillation of the free electrons along and perpendicularly to the long axis of the rods [1]. GNRs have attracted the most attention because of their high absorption cross sections and that their longitudinal surface plasmon resonance (LSPR) of GNRs can be fine tuned over the visible to near-infrared region by adjusting their aspect ratio. This unique plasmonic property makes them became a good candidate for wide varieties of applications. They are used for improving absorption in photovoltaic devices [2] biological marking [3] disease diagnosing and detecting [4, 5] or destroying cancer cells by photothermal effects [6, 7] Moreover, the increase in the intensity of the surface plasmon resonance absorption results in an enhancement of the electric field and surface enhanced Raman scattering of

molecules adsorbed on GNRs [8], etc. In addition, high absorption cross sections of GNRs facilitates efficiently energy absorption in the NIR region, allowing equally efficient conversion of the absorbed energy to thermal energy, which makes GNRs be more appropriate than gold nanoshells in photothermal effects.

Up to now, there have been many approaches studying on the synthesis of GNRs. A common top down technique to prepare GNRs is electron beam lithography [9]. This method has the advantage of preparing highly monodispersed NRs but it can only create a 2-dimensional structure in a single step and the instrumentation is expensive. As for bottom up techniques, there are two different methods for the synthesis of gold nanorods. One is using hard templates to physically confine the growth such that gold ions are only reduced inside this template. This method creates monodispersed gold particles and can control the shape and size of the NRs with the growth mechanism elucidated. But large scale synthesis is limited since it requires nonporous templates. In the other method, the gold ions are reduced in the presence of stabilized materials which bind to the surface of growing nanoparticle to direct the formation of NRs. As for the reduction path, we can choose one of the ways including photochemistry (UV-irradiation) [10], electrochemistry bio-reduction [11], or chemical reduction [12, 13]. Chemical reduction method is a simple, fast and economical method. By this way, Murphy and co-workers have fabricated gold NRs by using seed-mediated method [12]. The method consisted of two steps: In the first step, the ultrafine gold colloids with diameter 1–3 nm (named as gold seeds) were synthesized by reducing of chloroauric acid with a strong reducing agent (such as sodium borohydride). In the second step, the seeds were developed in growth solution containing chloroauric acid, cetyl trimethylammonium bromide (CTAB), cyclohexane and acetone in the presence of catalytic  $\text{Ag}^+$  and weak ascorbic acid. The size and shape of the GNRs were determined by various experimental parameters that affect the growth mechanism [12, 13]. The role of those parameters in growth solution in the synthesis of NRs has been extensively discussed [3, 13]. In the present work, the GNRs were synthesized via a seed-mediated method by varying the  $\text{Ag}^+$  concentration in the formation of the GNRs. The photothermal conversion effects of the GNRs have been proved by illuminating into the chicken tissues injected GNRs with the difference laser density power at wavelength of 808 nm.

## **2. EXPERIMENTAL**

### **2.1. Materials**

Sodium borohydride  $\text{NaBH}_4$ , gold (III) chloridetrihydrate  $\text{HAuCl}_4 \cdot 3\text{H}_2\text{O}$ , benzyl dimethylhexadecyl ammonium chloride (BDAC), and L-Gluthathione GSH were purchased from Sigma-Aldrich. Silver nitrate  $\text{AgNO}_3$  and L(+)-Ascorbic acid (AA) originates from China. Cetyl trimethylammonium bromide CTAB was supplied by AMRESCO. The heterobifunctional thiol PEG carboxylic acid (HS-PEG-COOH) was supplied by Creative Company. The bovine albumin serum (BSA) was purchased from Biochem. All chemicals were used without further purification, and Milli-Q water was used throughout this study.

### **2.2. Synthesis of GNRs by Seed-mediated method**

GNRs were synthesized by seed-mediated method using CTAB and BDAC in high concentrations as stabilizers for the formation of anisotropic shape of gold NPs. This method of fabrication consisted of two main stages: i) Synthesizing of seeds and ii) synthesizing of GNRs [11, 12].

### **2.3. Synthesizing of seeds**

Gold seed solution was prepared by mixing 10 mL CTAB 0.1 M solution with 125  $\mu$ L HAuCl<sub>4</sub> of 0.023 M, 0.6 ml ice-cold NaBH<sub>4</sub> 0.01M was injected to the above mixture under stirring, the solution colour changed from red to light brown, indicating the formation of gold nanoparticles (1-3 nm in diameter) appeared. Then, seed solution was kept at room temperature and used within 2-5 h.

### **2.4. Synthesizing of GNRs**

In order to consider role of Ag<sup>+</sup> in the formation of GNRs, 7 different samples of GNRs were prepared. Firstly, 150  $\mu$ l HAuCl<sub>4</sub> 0.023 mM was put into 10 ml of the mixture CTAB 0.1M and BDAC 0.005M in 7 different reactions. Then, various volumes of AgNO<sub>3</sub> corresponding to the Ag<sup>+</sup> concentrations of 0.0 mM; 0.024 mM; 0.040 mM; 0.048 mM; 0.064 mM; 0.080 mM; 0.107 mM; 0.134 mM were added in the above reaction solutions. Next, 25  $\mu$ l AA 0.25M reductant reaction agent was added. Finally, 100  $\mu$ l of the gold seed solution was put into each reaction solution under vigorous stirring at room temperature. The growth process of GNRs was maintained in 2 hours. The GNRs products were purified by centrifugation for 30 minutes at a speed of 14000 revolutions per minute and redispersed in deionized water. Then, GNRs were functionalized with biomolecules such as: heterobifunctional thiol PEG carboxylic acid (HS-PEG-COOH), glutathione (GSH) and bovine serum albumin (BSA) to prevent aggregation of GNRs after the removing of surfactant agents, and to form bioconjugate layers. The optical characteristics of the GNR solutions were recorded on a NIR-UV-2600 Shimadzu spectrophotometer; the morphology of GNRs as morphology means size and shape were observed through TEM Model Jem JEOL 1010 microscope.

### **2.5. Photothermal experiment**

Photothermal experiments of GNRs were realized by using laser diode at 808 nm, 2 W as light source. The laser light is coupled from the source to the tissue sample through an optical fiber 400  $\pm$  8  $\mu$ m in core diameter. The real tissue of chicken lean meat was used in this experience to investigate the thermal transfer of light. They were cut with 4x4x6 mm dimensions. To each samples, 0.25  $\mu$ l of GNR solution with optical density 10 at 800 nm wavelength was injected. The reference tissue sample was not injected with GNRs. The samples were then placed directly onto a surface of sensor PT100-CRZ. Laser power was determined by using the energy probe LM-3HTD of Coherent before use. The density powers of laser used for illuminating were 2; 4, and 6 W.cm<sup>2</sup>. The laser beam diameter on the sample was of about 8 mm. The temperature increase of the samples was carried out according to a similar process in the same time period. The temperature of the sample was recorded through changing resistance of the sensor whose output was connected to DAQ connected to a computer.

## **3. RESULTS AND DISCUSSION**

### **3.1. Effect of Ag<sup>+</sup> concentration on the formation of GNRs**

The study on synthesis of GNRs showed that the concentration of Ag<sup>+</sup> ions in growth solution was one of the factors that significantly affected the morphology of GNPs [3]. The research results of Huang *et al.* [14] showed that, in the synthesis of GNRs via the denatured

polyol method, the increase in concentration of  $\text{Ag}^+$  ions as well as gold crystals also changed gradually the morphology from octahedral into truncated octahedra, cube, etc.

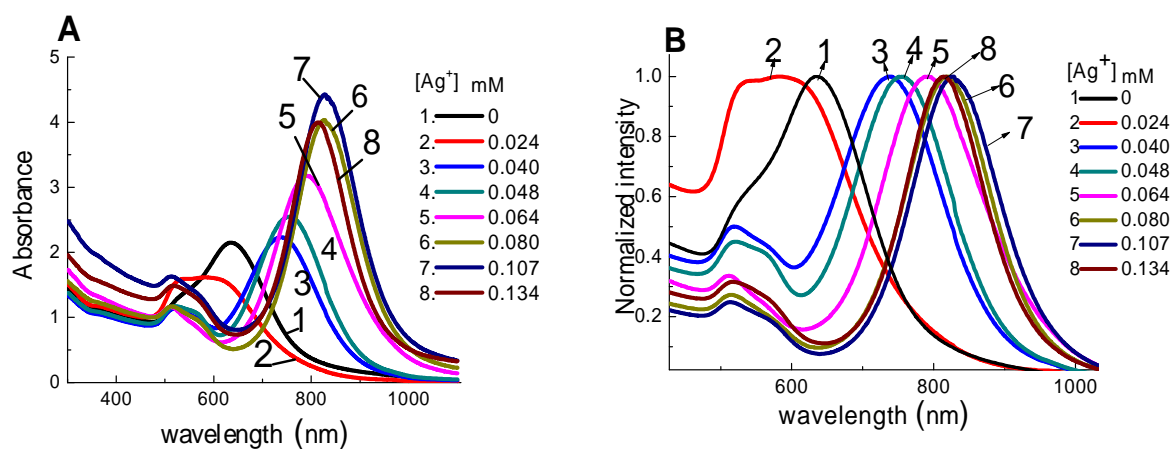


Figure 1. (A) The absorption spectra of the GNR solutions prepared under different  $\text{Ag}^+$  concentrations, and (B) their normalized absorption spectra.

Figure 1 shows absorption and normalized absorption spectra of the GNR solutions depending on the concentration of  $\text{Ag}^+$  ions. Without  $\text{Ag}^+$  ions and  $\text{Ag}^+$  concentration below of 0.04 mM in growth solution, the results shows that the absorption spectra obtained from these samples have only a maximum peak in the range of 500-600 nm, which characterizes the absorption of spherical gold nanoparticles. When the concentration of  $\text{Ag}^+$  ions were used in the range from 0.04 mM to 0.134 mM, the plasmon absorption spectra of these GNRs solution exhibit two absorption maximum corresponding to the oscillation of the free electrons along and perpendicular to the long axis of the rods. The transverse mode (transverse surface plasmon peak: TSP) shows a resonance at 515 nm and peak intensity almost constant, while the resonance of the longitudinal mode (longitudinal surface plasmon peak - LSP) increases from 603 nm to 830 nm and the intensity peaks increases from 1.59 to 4.42 for  $\text{Ag}^+$  concentration increasing up to 0.107. However, when that concentration further increased, i.e. from 0.107 mM to 0.134 mM, the intensity of LSP peak was reduced and blue shifted (Figure 1). Figure 1.b presents the normalized absorption spectra of the GNR solutions with second peak show that when the  $\text{Ag}^+$  concentration increases, there is a sharply red shift of the second absorption peak and the relative intensity of the first absorption peak decreases. In other words, changing the  $\text{Ag}^+$  concentration will influence on the LSP and on R- the ratio of LSP to TSP as shown in Figure 2. The line connecting the black squares shows the dependence of the LSP and the line connecting the triangles shows the dependence of the ratio of LSP to TSP on the  $\text{Ag}^+$  concentration. Figure 2 shows that when the  $\text{Ag}^+$  concentration increases from 0.04 mM to 0.107 mM, the both of longitudinal surface plasmon resonance ( $\lambda_{\text{mLSPR}}$ ) and the ratio of longitudinal surface plasmon resonance to transverse surface plasmon resonance (R) of GNR solutions increase. However, with further increase of this concentration, both of R and  $\lambda_{\text{mLSPR}}$  decrease. This result is coincided with those of the reference [15] and indicates that when the  $\text{Ag}^+$  concentration is between 0.08 mM and 0.107 mM, the aspect ratio of GNRs and the quantity of GNRs is the highest. The role of the  $\text{Ag}^+$  ion in the formation of GNRs is clear. When the  $\text{Ag}^+$  concentration is below of 0.024 mM, the GNRs are not formed. By adjusting the  $\text{Ag}^+$  concentration that allow us adjust the aspect ratio of the GNRs as well as the efficiency of the GNRs formation.

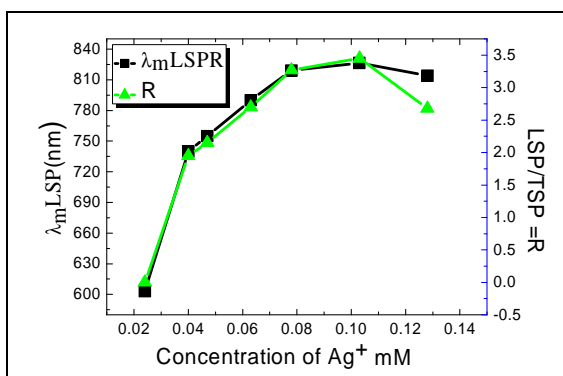


Figure 2. Dependence of LSP (squares) and R (triangles) of the GNRs on the Ag<sup>+</sup> concentrations.

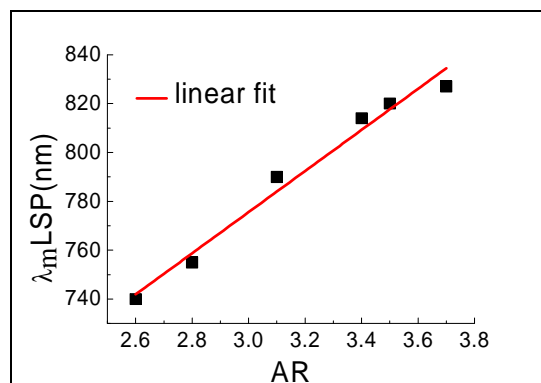


Figure 3. Dependence of the SPR maximum wavelength on the aspect ratio AR of the GNRs.

Figure 3 presents the linear relation between SPR wavelength and the aspect ratio of GNRs. As the AR increases, the SPR maximum is linearly red shifted. This optical property of the GNRs is different from that of GNSs for which the SPR only slightly shifts with the increase of the particle size. The dependence of SPR wavelength on the AR has been proved by Link *et al.* [16] using Gans theory. The dependence of the SPR maximum wavelength on the aspect ratio, AR, of GNRs and dielectric constant of the contacting medium can be expressed by the equation:

$$\lambda_{mLSPR} = (33.34AR - 46.31) \epsilon_m + 472.31$$

where  $\epsilon_m$  is the dielectric constant of the CTAB solution after synthesizing of GNRs. Correlation of  $\epsilon_m$  with CTAB concentration has also been identified by Iwunze *et al.* [17]. These results can be verified by observing the TEM images.

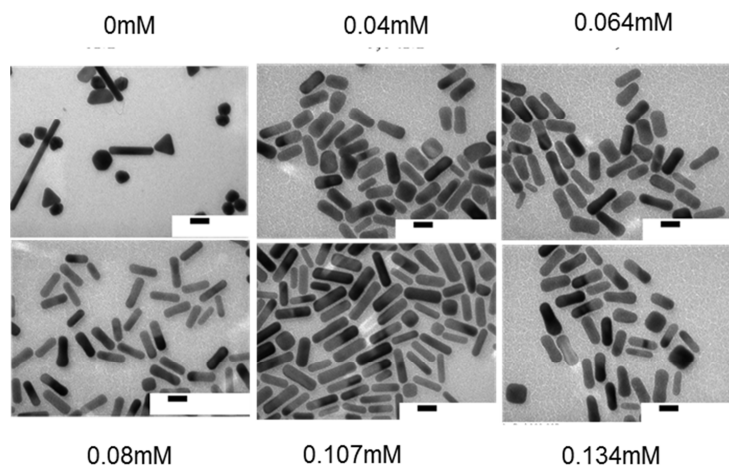


Figure 4. TEM images of the GNR solutions upon changing of the Ag<sup>+</sup> concentrations, at scale bare of 20 nm.

Figure 4 shows TEM images of the GNRs prepared under different Ag<sup>+</sup> concentrations as: 0 mM; 0.04 mM; 0.064 mM; 0.08 mM; 0.107 mM, and 0.134 mM. We can easily see that the yield of the rod and their uniformity increase while the diameter of the particles decreases as the Ag<sup>+</sup> concentration increases from 0.04 mM to 0.107 mM. Without Ag<sup>+</sup> ions, TEM image

indicates that the obtained sample contains different shapes, including spherical, triangle and a few high aspect ratio rod-like particles. This is consistent with results published in the ref. [4]. The quantity and length of GNRs increases proportionally with the  $\text{Ag}^+$  concentration added in the growth solution. However, when the  $\text{Ag}^+$  concentration is over 0.107 mM, the aspect ratio and the yield decrease. This result is consistent with the statement by Nikoobakht and El-Sayed [13]. So, there is a fit between the TEM images and UV-Vis/near infrared spectra, which also shows a tightly relation of the LSP absorption maximum with AR and between R and the yield of GNRs formation.

The general mechanism of GNR growth can be expressed according to the schematic in Figure 5 [18]. The mechanism starts with the crystal structure of the seeds. Then, preferential links of groups on the various crystal surfaces of seeds. Finally, the addition of metal ions on preferential crystal faces leads to the growth of GNRs.

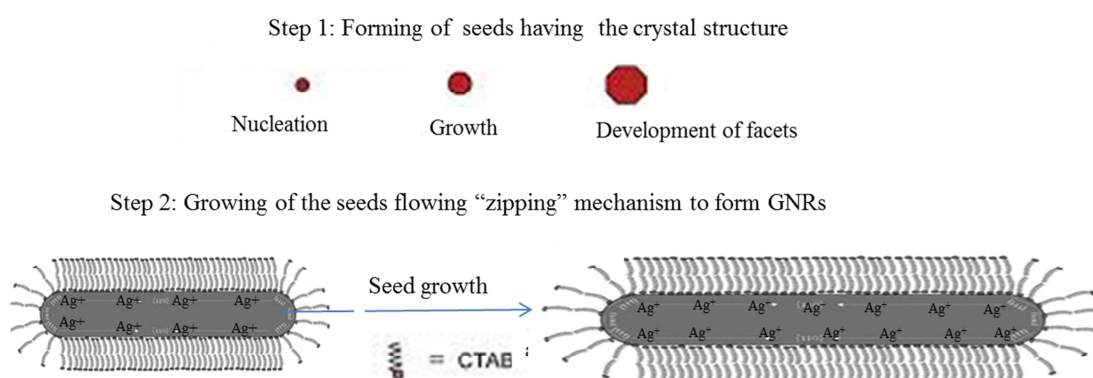


Figure 5. Schematic of the mechanism of GNR growth synthesized by the seed-mediated method.

Murphy *et al.* [18] supposed that the  $\text{CTA}^+$  headgroup binds to the side surface with some preference. This assumption stems from the fact that the distance between Au atoms on the side faces is more comparable to the size of the  $\text{CTA}^+$  headgroup than that of Au atoms on the (111) face at both ends of the GNRs (planar density of (110), (100) and (111) are 0.555, 0.785 and 0.907, respectively). By binding of  $\text{CTA}^+$  headgroups, the side faces have relatively large surface energy and become more stable. This leads to the growth in the two ends of nanorods along the [110] common axis on (111) faces and these faces do not contain  $\text{CTA}^+$  headgroups.  $\text{Ag}^+$  ions join to provide soft template for formation of rod which are formed by surface molecules as CTAB and BDAC. This has also been explained clearly by Kyoungweon Park [19]. Here,  $\text{Ag}^+$  ions link to  $\text{Br}^-$  ions in molecules CTAB leading to the fact that repulsion of molecules CTAB side along (110) crystal surface is reduced. In the same time, create weak links  $\text{Ag-Cl}$  in BDAC on (111) crystal surfaces at both ends of the soft template. Strong bonds pair  $\text{CTA-Ag-Br}$  acting as stabilizers inhibit the growth in the sides so it plays the role in creating anisotropy soft template. This allows the  $\text{Au}^{3+}$  to develop and prolong mainly at the both ends of gold NPs to generating GNRs. Stability and length of the template is proportional to the concentration of  $\text{Ag}^+$ . This explains why once the  $\text{Ag}^+$  concentration increases, the templates are more stable. Simultaneously, the development of the particles horizontally is inhibited to create more uniform NRs. Thus, when increasing the  $\text{Ag}^+$  concentration, it will promote the anisotropic development of seeds. The result is to increase the aspect ratio AR of the GNRs. However, when

the  $\text{Ag}^+$  concentration continues to grow, at the ends of the GNRs, which are protected by the presence of links CTA-Ag-Br. This prevents the anisotropic development of the gold seeds, therefore AR will not rise any further. So,  $\text{Ag}^+$  ions play an indispensable role in the synthesizing of GNRs. The presence of  $\text{Ag}^+$  increases yield of growth of GNRs. Also, by controlling the concentration of  $\text{Ag}^+$  in the range from 0.08 mM to 0.134 mM, the AR of the GNRs is the largest.

### 3.2. Binding GNRs with bio – molecules

Owing to the strong binding between thiols to noble metals, the HS-PEG-COOH, BSA, and GSH molecules, thiol containing molecules were used to stabilize the gold NPs. when GNRs were coated with these biomolecules their SPR spectra shapes almost had no change but their SPR intensity was increased from 5 to 10 percent (Fig. 6A). In addition, their LSP peaks are slightly red-shift, i.e. of about 4-14 nm ( $\Delta\lambda_m = 14, 9$  and 4 nm for GNRs @BSA, GNRs @GSH, and GNRs@PEG, respectively), as showed in Fig. 6B. These results are consistent with our previous studies [20, 21] It showed that these molecules are successfully conjugated with GNRs.

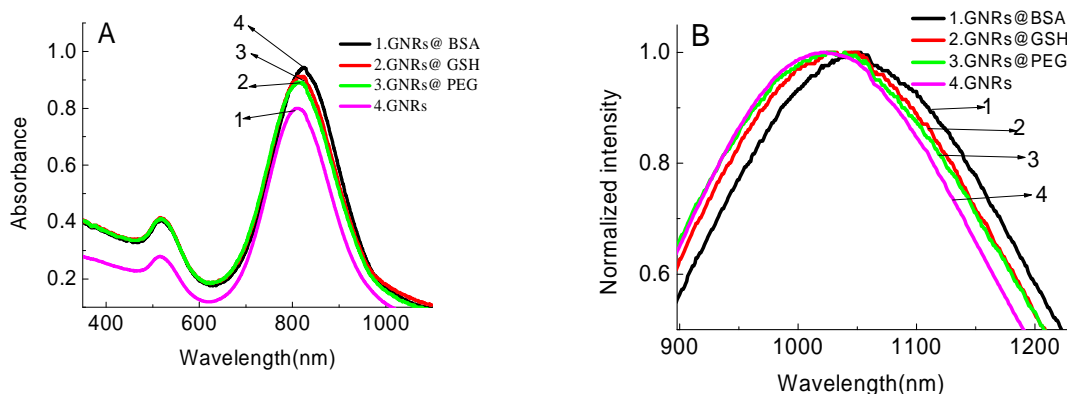


*Figure 6.* The absorption (A) and normalized absorption spectra (B) of the GNR solutions before and after binding with bio - combative molecules: BSA, GSH, PEG.

### 3.3. Photothermal applications

Figure 7 shows the increase of temperature of the same chicken tissues injected of 0.25  $\mu\text{l}$  of the GNR solution optical density 10 at 808 nm, and illuminated with different laser power densities of 2, 4, 6  $\text{W}/\text{cm}^2$  for about 10 minutes. The result shows that the temperature of tissue increases immediately and reaches thermal equilibrium after 30 seconds. At the temperature equilibration, the temperature difference of the sample increases from 15-23  $^{\circ}\text{C}$  corresponding to the power density of the laser source varying in the range of 2-6  $\text{W}/\text{cm}^2$ , as shown in Figure 7. The equilibrium is achieved when there is a balance between endothermic rate and exothermic rate into the environment. When the light turns off, the temperature of tissue reduces to room temperature. The mechanism of this effect follows the energy balance model presented in details in the reference [7]. From the obtained results, it can be seen clearly that the temperature of the tissue sample depends on the power density of the laser source. Figure 8 shows the temperature elevation of the sample ( $\Delta T$ ) is almost linear with the power density (I). This is consistent with the results published in our earlier paper [22]. According to this paper, the temperature of the

tissue sample increases by accumulating heat of many GNRs. Meanwhile, the temperature increase on the surface of an individual GNR in medium is given by the equation (1).

$$\Delta T_{\text{GNR}} = \frac{I \sigma_{\text{abs}}}{4 \pi k_0 R_{\text{eq}} \beta} \quad (1)$$

where  $\sigma_{\text{abs}}$  is absorption cross section of GNRs ( $\text{cm}^2$ );  $I$  is power density of laser beam ( $\text{W} \cdot \text{cm}^{-2}$ );  $R_{\text{eq}}$  is equivalent radius of a sphere with the same volume as the GNR (m),  $k_0$  is thermal conductivity of the surrounding medium,  $\beta$  is thermal capacity coefficient dependent on AR of GNRs by the formula (2).

$$\beta = 1 + 0.96586 \cdot \ln^2(\text{AR}) \quad (2)$$

Thus, the temperature of the system increases almost linearly with the power density.

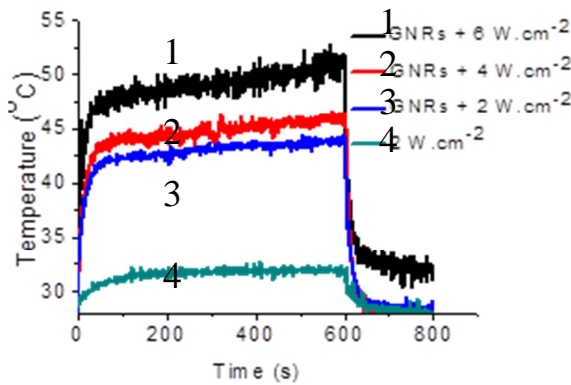


Figure 7. Temperature of the tissues injected GNR solution when illuminated by 808 nm infrared laser with different power density as a function of time. The measurements were taken at room temperature of 28 °C.

Figure 8. The temperature variation of the tissues injected GNR solution when illuminated by 808 nm infrared laser as a function of power density.

Also, the photothermal conversion efficiency can be calculated by the formula (3) [7, 22].

$$\eta = \frac{Q_{\text{abs}} - Q_{\text{surr}}}{P} \quad (3)$$

where  $h$  is the heat transfer coefficient,  $h_{\text{AuNR}} = 14.65 \text{ mW}/\text{cm}^2 \cdot \text{K}$  [23];  $S$  is the surface area of the tissue sample, in the experiment, a part of the tissue injected GNRs is regarded as a cylindrical with a diameter of 0.15 cm and a height of 0.4 cm.  $\Delta T$  is the temperature difference of the sample and the environment when the equilibrium is established. In case of the power density  $I$  is  $6 \text{ W}/\text{cm}^2$ , the laser power  $P$  equal to 0.106 mW (diameter of the spot on the tissue is 1.5 mm). The absorbance of the GNRs at 808 nm  $A_\lambda$  is 10.  $Q_{\text{surr}}$  expresses the heat dissipated from the light absorbed by the tissue during excitation time of 600 s.  $Q_{\text{surr}} = c \cdot m \cdot \Delta T / t = 0.02 \text{ mW}$  (in tissues, water accounts for 79 % of the volume, thus, the density of tissue is considered the density of water  $D = 1000 \text{ kg}/\text{m}^3$ , specific heat of tissue is considered specific heat of water,  $c = 4200 \text{ J}/\text{kg} \cdot \text{K}$ .  $\Delta T$  is the temperature change of the reference sample – Figure 7). Based on the equation (3), the photothermal conversion efficiency of GNRs excited by the light laser with the power density of  $6 \text{ W}/\text{cm}^2$   $\eta$  is 25.56 %.

#### 4. CONCLUSION

We have presented shortly about the successful fabrication of the GNRs by the seed-mediated method in the presence of  $\text{Ag}^+$ . The results show that the obtained GNRs are mono-dispersed in solution with uniform size. By adjusting the  $\text{Ag}^+$  concentration in the growth solution, the plasmon resonance absorption peaks of the GNR solutions can be tunable throughout the visible and near-infrared region of the spectrum as a function of  $\text{Ag}^+$  concentration. The role of  $\text{Ag}^+$  ions in the GNRs formation has been clarified. Further research will aim to create the GNRs with greater aspect ratio and to study binding of particles with biological molecules for applications in biomedicine. The photothermal effects of our GNRs were also tested in chicken tissue. The temperature of the sample increased almost linearly from 15-23 °C, corresponding to power density of the source increasing in the range from 2-6 W/cm<sup>2</sup>.

*Acknowledgements.* We acknowledge the funding from project VAST.CTVL.02/17-18.

#### REFERENCES

1. Kelly K.L., Coronado E., Zhao L.L., Schatz G. C. - The Optical Properties of Metal Nanoparticles: The Influence of Size, Shape, and Dielectric Environment, *J. Phys. Chem. B* **107** (3) (2003) 668–677.
2. Ghosh B., Espinoza-González R. - Plasmonics for Improved Photovoltaic Devices, *Juniper Online J. Mater. Sci.* **1** (2) (2007) 1-7.
3. Sisco P. N. (thesis) - Gold nanorods: Applications in chemical sensing, biological imaging and effects on 3-dimensional tissue culture, University of Illinois at Urbana-Champaign, 2010.
4. Agasti S. S., Rana S., Park M. H., Kim C. K., You C. C., Rotello V. M. - Nanoparticles for detection and diagnosis, *Adv. Drug Deliv. Rev.* **62** (3) (2010) 316-328.
5. Tong L., Wei Q., Wei A., and Cheng J.-X. - Gold nanorods as contrast agents for biological imaging: optical properties, surface conjugation and photothermal effects, *Photochem. Photobiol.* **85** (1) (2009) 21-32.
6. Huang X., Jain P. K., El-Sayed I. H, and El-Sayed M. A. - Plasmonic photothermal therapy (PPTT) using gold nanoparticles, *Lasers Med. Sci.* **23** (3) (2008) 217-228.
7. Richardson H. H., Carlson M. T., Tandler P. J., Hernandez P., Govorov A. O. - Experimental and Theoretical Studies of Light-to-Heat Conversion and Collective Heating Effects in Metal Nanoparticle Solutions, *Nano Lett.* **9** (3) (2009) 1139-1146.
8. Tian F., Bonnier F., Casey A., Shanahan A. E., Byrne H. J. - Surface enhanced Raman Scattering with gold Nanoparticles, *Anal. Methods.* **6** (22) (2014) 9116-9123.
9. Shalaev V. M., Cai W., Chettiar U. K., Yuan H. K., Sarychev A. K, Drachev V. P., Kildishev A. V. - Negative index of refraction in optical metamaterials, *Optics Letters* **30** (24) (2015) 3356-3358.
10. Niidome Y., Nishioka K., Kawasaki. H., Yamada S. - Rapid synthesis of gold nanorods by the combination of chemical reduction and photoirradiation processes; morphological changes depending on the growing processes, *Chem. Commun.* (18) (2003) 2376-2377.
11. Canizal G., Ascencio J. A., Gardea-Torresday J., Yacamán M. J. - Multiple twinned gold nanorods grown by bio-reduction techniques, *J. Nanoparticle Res.* **3** (5) (2001) 475-481.

12. Jana N. R., Gearheart L., Murphy C. J. - Seed-Mediated Growth Approach for Shape-Controlled Synthesis of Spheroidal and Rod-like Gold Nanoparticles Using a Surfactant Template, *Adv. Mater.* **13** (18) (2001) 1389-1393.
13. Nikoobakht B., and El-Sayed M. A. - Preparation and growth mechanism of gold nanorods (NRs) using seed-mediated growth method, *Chem. Mater.* **15** (10) (2003) 1957–1962.
14. Huang X., Jain P. K., El-Sayed I. H., El-Sayed M. A. - Gold nanoparticles: from synthesis and properties to biological and biomedical applications, *Nanomed.* **2** (5) (2007) 681-693.
15. Huang X., Neretina S., El-Sayed M. A. - Gold nanorods: from synthesis and properties to biological and biomedical applications, *Adv. Mater. Deerfield Beach Fla.* **21**(48) (2009) 4880-4910.
16. Link S., Mohamed M. B., and El-Sayed M. A. - Imulation of the Optical Absorption Spectra of Gold Nanorods as a Function of Their Aspect Ratio and the Effect of the Medium Dielectric Constant, *J. Phys. Chem. B* **103** (16) (1999) 3073–3077.
17. Iwunze M. O. - The determination of the effective dielectric constant of micelles and microemulsions, *Phys. Chem. Liq.* **43** (2) (2005) 195-203.
18. Murphy C. J., Sau T. K., Gole A. M., Orendorff C. J., Gao J., Gou L., Hunyadi S. E., and Li T. - Anisotropic Metal Nanoparticles:□ Synthesis, Assembly, and Optical Applications, *J. Phys. Chem. B.* **109** (29) (2005) 13857–13870.
19. Park K. (thesis) - Synthesis, Characterization, and Self –Assembly of Size Tunable Gold Nanorods, Georgia Institute of Technology (2006).
20. Nghiem Thi Ha Lien, La Thi Huyen, Vu Xuan Hoa, Chu Viet Ha, Nguyen Thanh Hai, Le Quang Huan, E. Fort, Do Quang Hoa, Tran Hong Nhung - Synthesis, capping and binding of colloidal gold nanoparticles to proteins, *Adv. Nat. Sci. Nanosci. Nanotechnol.* **1** ( 2) (2010) 025009.
21. Nghiem Thi Ha Lien, Nguyen Thi Tuyen, Fort E., Nguyen Thanh Phuong, Hoang Thi My Nhung, Nguyen Thi Quy, Tran Hong Nhung - Capping and *in vivo* toxicity studies of gold nanoparticles, *Adv. Nat. Sci. Nanosci. Nanotechnol.* **3** (1) (2012) 0015002.
22. Vu Thi Thuy Duong, Tran Thi Thuong, Nghiem Thi Ha Lien, Do Quang Hoa, Tran Hong Nhung - The light- to- heat Conversion of Gold Nanoshells and Nanorods in tissue, *Commun. Phys.* **24** (3S2) (2016) 85-90.
23. Tian Q., Jiang F., Zou R., Liu Q., Chen Zh., Zhu M., Yang Sh., Wang J., Wang J., Hu J.- Hydrophilic Cu<sub>9</sub>S<sub>5</sub> Nanocrystals: A Photothermal Agent with a 25.7 % Heat Conversion Efficiency for Photothermal Ablation of Cancer Cells in Vivo, *ACS Nano* **5** (12) (2011) 9761-9771.